Effects of the ratio of sphere size to laser focal spot on the dominant in-band EUV emitting region

Sam Yuspeh*, Kevin L. Sequoia, Yezheng Tao, Mark S. Tillack, Russell A. Burdt and Farrokh Najmabadi

Department of Electrical and Computer Engineering and the Center for Energy Research, University of California San Diego, 9500 Gilman Drive, La Jolla, Ca 92093-0407

ABSTRACT

Previous experiments on Nd:YAG laser produced Sn plasmas showed little dependence of the location of the dominant in-band extreme ultraviolet emitting region on target geometry. Modeling and experiments were preformed in order to better understand this phenomenon. A two-dimensional radiation hydrodynamic code, h2d, was benchmarked with experiments using Sn microspheres. Numerically obtained densities above the diagnostic limitation and temperature profile maps, which cannot be measured experimentally, were used to explain the effect, which comes from a relatively small change in the location of the critical density surface. This is important to EUV lithography because both the density and temperature play significant roles in the generation and transport of in-band EUV light. It is desired to have the highest possible density at the dominant emitting surface and the smallest possible surrounding plasma to produce high 13.5 nm conversion efficiency (2% bandwidth). The target geometry impacts the amount of lateral expansion leading to dramatically different density profiles and therefore can be optimized to meet these conditions.

Keywords: Laser produced plasma, Ultraviolet sources, Tin, Radiation hydrodynamic model

1. INTRODUCTION

One factor limiting the minimum node size of semiconductor microchips is the wavelength used for optical lithography. Currently 193 nm light is being used but a shorter wavelength light is required to produce smaller features. Extreme ultraviolet (EUV) lithography (EUVL) is likely to be the next generation technology for high volume manufacturing of semiconductors with features 32 nm and below.[1] One of leading candidates for EUVL sources is laser produced Sn plasma (LPP) due to the potential high conversion efficiency (CE) from laser to 13.5 nm (2% bandwidth) EUV light. One of the major costs of an EUVL system is the laser; therefore, an increase in CE reduces the cost of ownership of the system. To meet the high power demands of the EUVL system, it is more cost effective to increase the laser frequency than the laser energy. While the geometric shape of the target can be a key factor in the CE, a droplet generator will most likely be used to produce spherical targets at 10 kHz. As a result, it makes spherical target geometry of the utmost importance. It has been shown that the ratio of the sphere diameter to laser full width half maximum (FWHM) focal spot size (SD/FSS) significantly affects the plasma expansion and CE.[2]

Diagnostics are able to reliably measure the plasma electron density[3], ion emission[4], spectra[5] and image the in-band emission region[6] for Sn LPP. However, many of the techniques that are used to measure plasma temperatures, such as Thomson Scattering, cannot be applied here due to the small size and steep gradients in temperature and density of the plasma. Not only does the density but also the temperature play an important role in the generation and transports of the in-band EUV light through re-absorption. A two-dimensional radiation hydrodynamic code h2d is used to generate electron density, temperature and laser absorption profile maps for varying SD/FSS ratio at typically commercial EUV system parameters.[7] There has been Sn LPP previously modeled with Hyades[8], a one dimensional version of h2d, but the

* syuspeh@ucsd.edu

Alternative Lithographic Technologies, edited by Frank M. Schellenberg, Bruno M. La Fontaine
Proc. of SPIE Vol. 7271, 727136 · © 2009 SPIE · CCC code: 0277-786X/09/$18 · doi: 10.1117/12.814167

work presented here is the first benchmarking of the h2d for EUV applications. This paper shows a brief comparison between experimental results and h2d modeling, a review of previous SD/FSS ratio work and use the h2d result to further explain why the dominant in-band EUV emitting region (DER) is independent of the target geometry.

2. BENCHMARKING

2.1 Experimental paramaters

The targets are fabricated by sputter coating ~2-3 μm of 5N pure Sn onto glass beads with varying diameters. The targets are heated by a 1.064 μm 8 ns FWHM laser that is referred to as the pump laser. The pump laser is focused to a Gaussian spot size of 80 μm FWHM with energy of 250 mJ. A 532 nm 130 ps laser is employed as the probe laser. The probe laser passes through the plasma perpendicular to the pump laser. The electron density is then calculated by the phase shifts of the probe beam observed by a Nomarski interferometer. Additional experimental set-up is discussed by Tao *et al*.[9]

2.2 h2d Paramaters

The radiation hydrodynamic physics of h2d is the same as HYADES- both using a three-temperature model. The model is operated using an average-atom local thermal equilibrium (LTE) for the atomic physics and a tabular equation of state derived from the Los Alamos National Laboratory (LANL) T4 SESAME tables for the radiation transport. Rosseland mean opacities are used for flux-limited gray radiation diffusion. The geometry of the target is the same as the experiment with a glass inner shell and 2 μm of Sn coating. There are approximately 30 zones in the azimuthal direction and 50 zones feathered towards the outside in the radial direction with the smallest zone about 1 nm thick. Additional information about the HYADES code is presented elsewhere.[10]

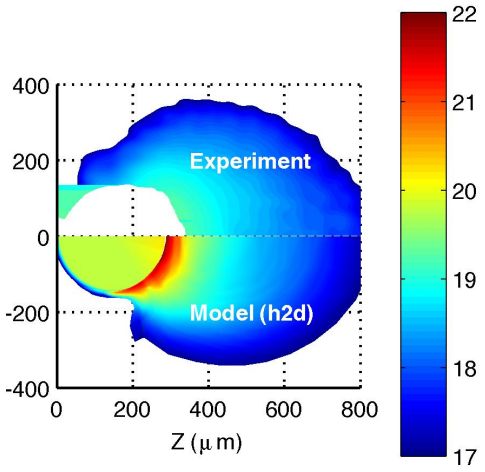

FIG. 1. Log_{10} of the electron density at the peak of the laser pulse for a typical experimental (top) and h2d simulation (bottom) 280 μm diameter sphere. The diagnostic limitation of the experiment is 10^{17}-10^{19} n_e cm^{-3}.

2.3 Experiment Vs. Modeling

The h2d electron density plots are compared to experimental recorded density at peak of the laser. The interferometer used in this experiment has a range of ~10^{17}-10^{19} n_e (cm^{-3}) with resolution better than 15 μm. The algorithm that is used to convert interferograms into density maps is discussed elsewhere.[11] A comparison between a typical experimentally recorded 280 μm diameter sphere density profile map at the peak of the laser is compared to the h2d model in Fig. 1 and

the electron density along the laser axis is shown in Fig 2. There is good agreement between the model and the experiment in both axes. It appears that the model has a slightly higher density than the experiment, which is most likely due to inability to match the exact conditions of the experiment and limitations of the code.

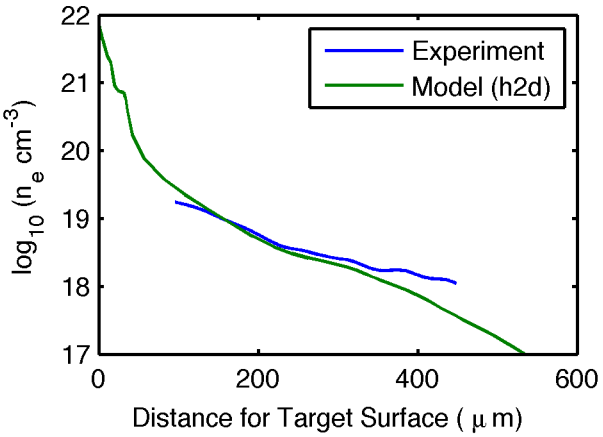

FIG. 2. The electron density along the laser axis for the experimental (blue) and h2d model (green) for a 280 μm diameter sphere.

The h2d model uses a perfect Gaussian spatial and temporal profile while that is not the case in the experiment. Any variation in the spatial or temporal shape of the laser could affect the amount and location of the laser absorption before the peak and thus lead to a slightly different electron density profile. The density map could also be affected by the ±0.5 ns jitter between the pump and probe laser. There are also several limiting factors in the code. The mesh size is somewhat limited due to the computational time required to complete the model. A smaller mesh should increase the resolution in the model and may lead to better agreement. Even though the model produces a higher density, the scale length of the model is slightly smaller than the experiment, 110 μm compared to 125 μm. The plasma scale length is calculated by fitting exponential decay function, $\exp(-x/l_s)$, to Fig. 2 which is the electron density along the laser axis where l_s is the plasma scale length. The scale length could be affected by the absence of atomic physics in the h2d model. Gray radiation is used for the emission and absorption in the model. However, it has been shown that the absorption coefficients change dramatically for different wavelengths in the EUV region for Sn.[12] Even with the slight discrepancies between the model and the experiment, h2d shows good agreement with the experiment and provides additional information that cannot be obtained experimentally.

3. RESULTS

3.1 Review of Previous SD/FSS work[2]

The plasma expansion is dependent on the SD/FSS ratio because the expansion is perpendicular to the target surface. Smaller spheres have a larger lateral component of plasma expansion due to larger angles between the target surface and the laser beam. Plasma lateral expansion transfers energy from inside the laser path to outside the laser path. This reduces the effective heating of the laser by wasting energy and also reduces the amount of material being heated by the laser. The electron density along the laser axis as a result is shifted towards the laser for larger SD/FSS ratios. However, the DER remains constant for all SD/FSS ratio, which is discussed later using h2d modeling results. The higher ion densities generate more in-band EUV and thus produce higher CEs. There exist four distinct CE regimes for SD/FSS ratios; a linear regime (below 1.6 SD/FSS ratio), a flat regime (1.6-2.25 SD/FSS ratio), a gain regime (2.25-2.5 SD/FSS ratio) and a saturation regime (above 2.5 SD/FSS ratio). In the linear regime, the laser beam overfills the target so as the size of the target increases so does the mass ablation, leading to an increase in CE. There are little changes in the plasma expansion in the flat regime creating a relatively flat CE. In the gain regime, a large jump in the CE occurs caused by

the reduction of lateral expansion to the point where the plasma remains inside the beam path. In the saturation regime, the plasma expansion changes very little but there is still some lateral component compared to a planar target.

3.2 Density & Laser Absorption

Figure 3 shows h2d models of the electron density maps at the laser peak for sphere diameters of 90 μm, 130 μm, 180 μm, 200 μm, and 280 μm corresponding to SD/FSS ratios of 1.13, 1.63, 2.25, 2.50 and 3.5, respectively. The differences in the electron density profile maps for varying SD/FSS ratios of h2d models are not as dramatic as the experimental results, which are caused by the large mesh size in the azimuthal direction. The modeling still shows a reduction in lateral expansion for larger size spheres. It should be noted that spheres that are smaller than or comparable to the beam size shows plasma expansion behind the target (Fig. 3a and Fig. 3b). The h2d models show shifts in the electron density at the diagnostic limit (10^{19} cm^{-3}) in Fig. 4 similar to the experimental results. The scale lengths are independent of the SD/FSS ratio, which is also seen in the experiment. It is shown in Fig. 4 that the critical density surface ($1.1*10^{21}$ cm^{-3}) is very close to the target surface leading to differences of less than 5 μm for all SD/FSS ratios. Laser absorption occurs over a wide range of densities from under dense plasma to the critical density.[13] The spatial location of the critical density impacts the laser absorption profile more than the actual density of the under dense plasma. As a result the peak laser absorption varies by less than 10 μm for all SD/FSS ratios due to the critical density having little variation with respect to the target surface, shown in Fig. 5. The size of the plasma affects the amount of EUV light being reabsorbed by the plasma itself but has little affect on the absorption of the laser.

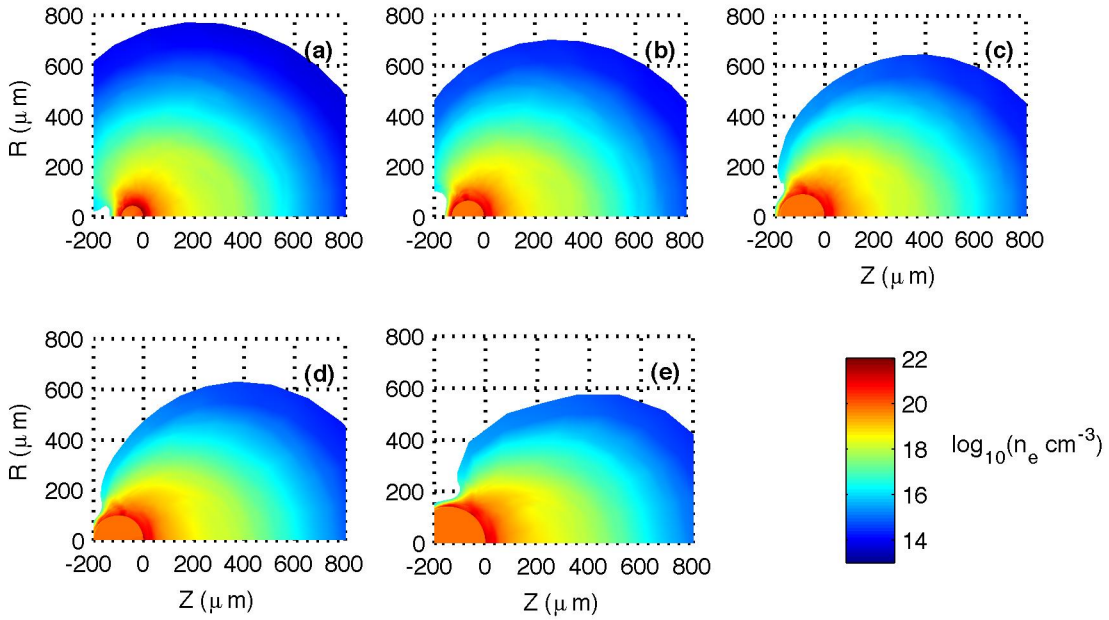

FIG. 3. The electron density at the peak of the laser for SD/FSS ratios of (a)1.13, (b)1.63, (c) 2.25, (d) 2.50 and (e) 3.50. The edge of the spheres are positioned at Z=0.

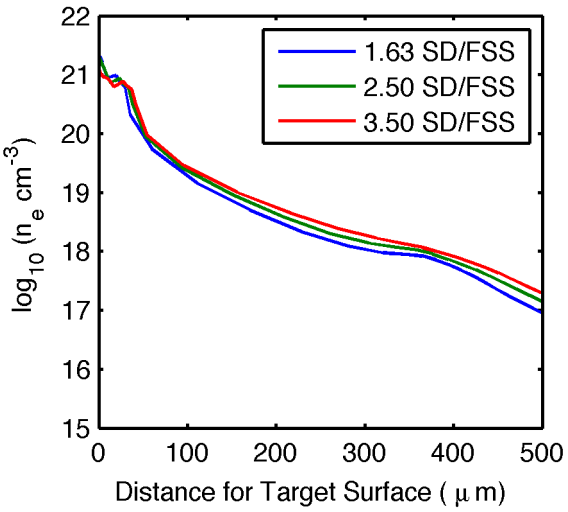

FIG. 4. The electron density along the laser axis at the peak of the laser for SD/FSS ratios of 1.63 (blue), 2.50 (green) and 3.50 (red).

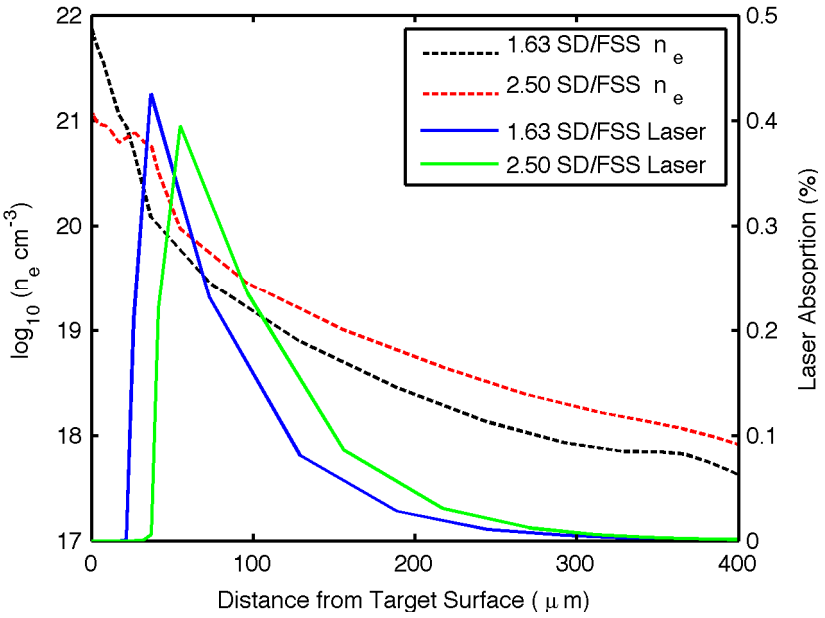

FIG. 5. The laser absorption along the axis at the peak of the laser pulse for SD/FSS ratios of 1.63 (blue) and 2.50 (green). Also plotted is the electron density for SD/FSS ratios of 1.63 (black dashes) and 2.50 (red dashes).

3.3 Temperature

There are many mechanisms affecting the electron temperature but three key factors are the laser absorption, the amount of material being heated and the energy transfer in the plasma. A small sphere has a lower density and similar laser absorption to a larger sphere, which would lead to a higher electron temperature. However, the small sphere has more lateral expansion thus reducing the total energy in the region where the laser is being absorbed. These three effects counteract each other leading to similar temperature profiles shown in Fig. 6. There are varying reports of the cutoff

temperature for in-band EUV generation ranging from 20-30 eV.[14-16] The high critical density of 1 μm lasers leads to the laser absorption and in-band EUV generation occurring at an optically thick (for in-band EUV) region of the plasma, which leads to the plasma being modeled as an inner region having a emitting surface (black body radiator) with a surrounding absorbing plasma.[17] Figure 7 shows the electron temperature along the laser axis for SD/FSS ratios of 1.63, 2.50 and 3.50. The cutoff temperature which corresponds to the emitting surface are all within 10 μm for all SD/FSS ratios leading to nearly identical DERs.

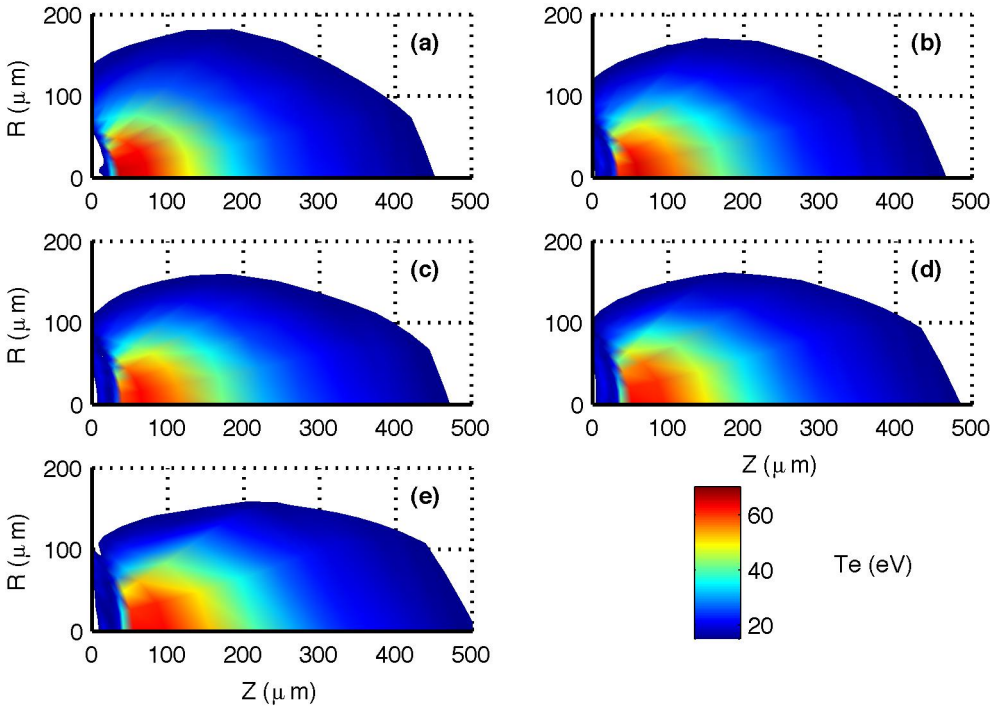

FIG. 6. The electron temperature at the peak of the laser for SD/FSS ratios of (a) 1.13, (b) 1.63, (c) 2.25, (d) 2.50 and (e) 3.50. The edge of the spheres are positioned at Z=0.

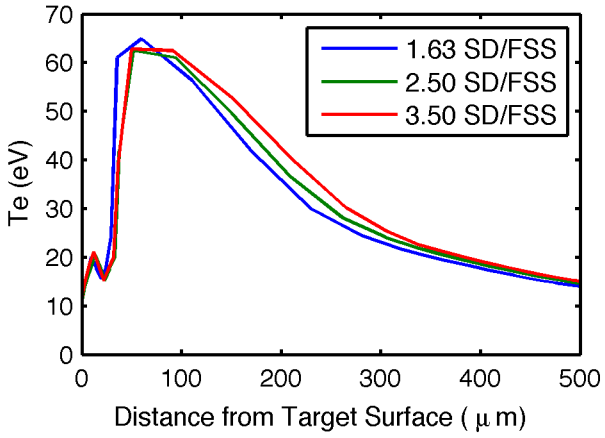

FIG. 7. The electron temperature along the laser axis at the peak of the laser for SD/FSS ratios of 1.63 (blue), 2.50 (green) and 3.50 (red).

4. CONCLUSION

Benchmarking of h2d for a 1 μm Sn LPP was shown to be in good agreement with experimental results. The changes in plasma shape were not as noticeable as the experiment for different SD/FSS ratios due to the relatively large mesh of the model. A reduction in the lateral expansion component of the plasma was noticed with an increase in sphere diameter. Shifts in the electron density along the laser axis were seen in both the experiment and h2d model. H2d was able to model electron densities above and below the diagnostic limit of the experiment. The critical density location varied from 2-7 μm away from the original target surface. The variation was small enough that it had little impact on the laser absorption profile. Similar laser absorption coupled with lower densities in the absorption region and an increase in energy being transferred out of the laser absorption region for smaller spheres lead to similar electron temperature profile. The similar electron temperature maps explained why previous experiments showed insignificant differences in the location of the DER for different SD/FSS ratios.

ACKNOWLEDGMENTS

The author would like to thank Rich Stephens and General Atomics for the use of the h2d simulation code. This work was supported by Cymer Inc., Extreme UltraViolet Lithography System Development Association (EUVA) and by the University of California (UC) under the UC Industry-University Cooperative Research Program (ele06-10278).

REFERENCES

[1] P. J. Silverman, "Extreme ultraviolet lithography: overview and development status," Journal of Microlithography, Microfabrication, and Microsystems **4**, 011006 (2005).

[2] S. Yuspeh, K. L. Sequoia, Y. Tao, M. S. Tillack, R. Burdt, and F. Najmabadi, "Optimization of the size ratio of Sn sphere and laser focal spot for an extreme ultraviolet light source," Applied Physics Letters **93**, 221503 (2008).

[3] Y. Tao, H. Nishimura, S. Fujioka, A. Sunahara, M. Nakai, T. Okuno, N. Ueda, K. Nishihara, N. Miyanaga, and Y. Izawa, "Characterization of density profile of laser-produced Sn plasma for 13.5 nm extreme ultraviolet source," Applied Physics Letters **86**, 201501 (2005).

[4] S. Fujioka, H. Nishimura, K. Nishihara, M. Murakami, Y. Kang, Q. Gu, K. Nagai, T. Norimatsu, N. Miyanaga, and Y. Izawa, "Properties of ion debris emitted from laser-produced mass-limited tin plasmas for extreme ultraviolet light source applications," Applied Physics Letters **87**, 241503 (2005).

[5] Y. Tao, S. S. Harilal, M. S. Tillack, K. L. Sequoia, B. O'Shay, and F. Najmabadi, "Effect of focal spot size on in-band 13.5 nm extreme ultraviolet emission from laser-produced Sn plasma," Optics Letters **31**, 2492 (2006).

[6] Y. Tao, H. Nishimura, T. Okuno, S. Fujioka, N. Ueda, M. Nakai, K. Nagai, T. Norimatsu, N. Miyanaga, and K. Nishihara, "Dynamic imaging of 13.5 nm extreme ultraviolet emission from laser-produced Sn plasmas," Applied Physics Letters **87**, 241502 (2005).

[7] J. Larson, in *h2d is a commercial product of Cascade Applied Sciences Incorporated, 6325 Trevarton Drive, Longmont, CO 80503. Electronic mail: larsen@casinc.com.*

[8] B. O'Shay, F. Najmabadi, S. S. Harilal, and M. S. Tillack, "Nanosecond spectroscopy of expanding laser-produced tin plasma," Journal of Physics: Conference Series **59**, 773 (2007).

[9] Y. Tao, M. S. Tillack, S. S. Harilal, K. L. Sequoia, and F. Najmabadi, "Investigation of the interaction of a laser pulse with a preformed Gaussian Sn plume for an extreme ultraviolet lithography source," Journal of Applied Physics **101**, 023305 (2007).

[10] J. T. Larsen and S. M. Lane, "HYADES. A plasma hydrodynamics code for dense plasma studies," Journal of quantitative spectroscopy & radiative transfer **51**, 179 (1994).

[11] L. B. Da Silva, T. W. Barbee, R. Cauble, P. Celliers, D. Ciarlo, S. Libby, R. A. London, D. Matthews, S. Mrowka, and J. C. Moreno, "Electron Density Measurements of High Density Plasmas Using Soft X-Ray Laser Interferometry," Physical Review Letters **74**, 3991 (1995).
[12] A. Sasaki, A. Sunahara, K. Nishihara, T. Nishikawa, K. Fujima, T. Kagawa, F. Koike, and H. Tanuma, "Atomic modeling of the plasma EUV sources," High Energy Density Phys. **3**, 250 (2007).
[13] J. S. De Groot, K. G. Estabrook, W. L. Kruer, R. P. Drake, K. Mizuno, and S. M. Cameron, "Distributed absorption model for moderate to high laser powers," Physics of Fluids B: Plasma Physics **4**, 701 (1992).
[14] T. Ando, S. Fujioka, H. Nishimura, N. Ueda, Y. Yasuda, K. Nagai, T. Norimatsu, M. Murakami, K. Nishihara, and N. Miyanaga, "Optimum laser pulse duration for efficient extreme ultraviolet light generation from laser-produced tin plasmas," Applied Physics Letters **89**, 151501 (2006).
[15] V. Bakshi, *EUV Sources for Lithography*. (SPIE Press, 2005).
[16] A. Cummings, G. O. Sullivan, P. Dunne, E. Sokell, N. Murphy, and J. White, "Conversion efficiency of a laser-produced Sn plasma at 13.5 nm, simulated with a one-dimensional hydrodynamic model and treated as a multi-component blackbody," J. Phys. D: Appl. Phys. **38**, 604 (2005).
[17] K. L. Sequoia, Y. Tao, S. Yuspeh, R. Burdt, and M. S. Tillack, "Two dimensional expansion effects on angular distribution of 13.5 nm in-band extreme ultraviolet emission from laser-produced Sn plasma," Applied Physics Letters **92**, 221505 (2008).